Geomechanics and Engineering, *Vol. 39, No. 2 (2024) 171-179*
https://doi.org/10.12989/gae.2024.39.2.171

Upper bound solution on seismic anchor force and earth pressure of a combined retaining structure

Yu-liang Lin*[1,4], Li Lu[1,4a], Hao Xing[2b], Xi Ning[2c] and Li-hua Li[3d]

[1]*School of Civil Engineering, Central South University, Changsha 410075, China*
[2]*The Fourth Engineering Co., Ltd., China Railway Seventh Group, Wuhan 430074, China*
[3]*Key Laboratory of Health Intelligent Perception and Ecological Restoration of River and Lake, Ministry of Education, Hubei University of Technology, Wuhan 430068, China*
[4]*Key Laboratory for Disaster Prevention and Mitigation of Rail Transit Engineering Structures of Hunan Province, Central South University, Changsha 410075, China*

(*Received December 16, 2023, Revised September 12, 2024, Accepted September 30, 2024*)

Abstract. Gravity wall combined with anchoring frame beam is widely adopted to support a high slope under complex geomorphic condition, in which the rigid gravity wall is adopted as a lower structure and the flexible anchoring frame beam serves as an upper structure. The seismic anchor force and the seismic active earth pressure are two essential issues for the seismic design of combined retaining structure in high seismic intensity area. In this study, an analytical model of combined retaining structure is established based on the upper bound theorem of limit analysis, and the formulas for seismic anchor force and seismic active earth pressure of combined retaining structure are derived. The results are optimized by using the global optimization algorithm. The proposed method is verified by a comparison with previous method. Moreover, the influence of main parameters on seismic anchor force and seismic active earth pressure is analyzed to facilitate the seismic design of such combined retaining structure.

Keywords: anchoring frame beam; gravity wall; seismic active earth pressure; seismic anchor force; upper bound theorem

1. Introduction

The gravity wall is a traditional easily-constructed and easily-accessed rigid structure that relies on its gravity to support the slope (Ahmed and Basha, 2021, Lee *et al*. 2023, Lim *et al*. 2023, Fu *et al*. 2020, Hwang and Chen 2011, Zhang *et al.* 2024). Nevertheless, the height of gravity wall is limited due to a high requirement of bearing capacity of foundation. The anchoring frame beam, as a flexible structure, is widely adopted for different kinds of slope as long as there is an adequate space for a certain slope angle (Lin *et al*. 2017, Hong *et al*. 2022, Bera 2014). The gravity wall combined with anchoring frame beam presents a rigid characteristic at lower stage, and a flexible characteristic at upper stage synchronously, which is more applicable for a high slope under complex geomorphic conditions (Lin *et al*. 2020a).

∗Corresponding author, Professor
E-mail: linyuliang11@csu.edu.cn
[a]Ph.D Candidate
E-mail: luli050@163.com
[b]Engineer
E-mail: m13089777884@163.com
[c]Engineer
E-mail: 419918375@qq.com
[d]Professor
E-mail: researchmailbox@163.com

The response of slope and supporting structure under earthquake loading is widely concerned in geotechnical engineering. Some scholars have studied the real response of retaining structures through shaking table test and numerical analysis (Lian *et al*. 2023, Zhou *et al*. 2023, Lin *et al*. 2020b, Yazdandoust *et al.* 2023). Lin *et al* (2018, 2022) obtained the acceleration amplification distribution and the anchor axial stress of an anchoring frame beam combined with a gravity wall or a sheet-pile wall by shaking table test and numerical simulation. Jo *et al*. (2017) observed the distribution of seismic earth pressure under different seismic loading through centrifuge test. The seismic design of retaining structures is generally conducted based on the pseudo-static method (Lee *et al*. 2019, Steedman and Zeng. 1990, Biondi *et al*. 2014, Lim and Jeong 2020, Karkanaki *et al*. 2019), in which the seismic loading is simplified as an inertial force which can be decomposed into horizontal and vertical directions. Thereafter, the conventional methods for evaluating the stability of a slope or retaining structures are mostly developed by combining the pseudo-static method with the limit equilibrium method (Greco 2014, Nouri *et al*. 2008, Shin 2023), the limit analysis method (Das *et al*. 2022, Kang *et al*. 2023, Lin *et al*. 2020c), the strength reducing method (Sun *et al*. 2021, Nian *et al*. 2016) and the Newmark method (Trandafir *et al*. 2009, Kokusho 2019, Zhang *et al*. 2021).

Research on stability of a slope supported by a single retaining structure under earthquake loading is widely

ISSN: 2005-307X (Print), 2092-6219 (Online)

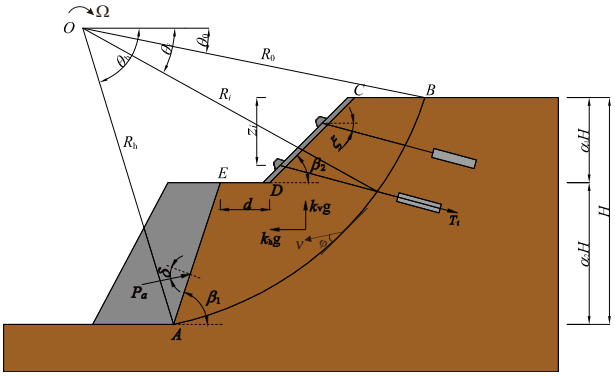

Fig. 1 The failure mechanism of combined retaining structure

reported (Li and Yang 2018, Zhao *et al*. 2016, Zhong and Yang 2021, Krabbenhoft 2018, Srikar and Mittal 2021). Nevertheless, the seismic behavior of a gravity wall combined with anchoring frame beam is different from that of a traditional rigid wall or a flexible retaining structure. It is important to deduce the seismic anchor force and the seismic active earth pressure of a gravity wall combined with anchoring frame beam under earthquake loading. The failure mechanism of gravity wall combined with anchoring frame beam is established based on upper bound theorem of limit analysis. Meanwhile, the effect of main parameters on seismic anchor force and seismic active earth pressure is analyzed to facilitate the seismic design of a gravity wall combined with anchoring frame beam.

2. Failure mechanism of combined retaining structure

It is likely that the potential sliding surface of a cohesive soil slope would present a log spiral characteristic. Consequently, the logarithmic spiral failure mechanism can improve the accuracy of upper bound solution compared with a plane surface for a cohesion soil slope (Chen *et al*. 1969, Lu *et al*. 2023). A failure mechanism of gravity wall combined with anchoring frame beam is established based on the upper bound limit theorem, as shown in Fig. 1. In which, a gravity wall serves as a rigid wall at lower stage, and an anchoring frame beam is a flexible structure at upper stage. The potential failure surface is assumed as a logarithmic spiral line that goes through Points A and B, which is expressed as $R(\theta) = R_0 \cdot e^{(\theta-\theta_0)\tan\varphi}$ within the polar coordinate system by taking Point O as an origin point. The potential sliding body $ABCDEA$ is assumed as a rigid plasticity since the limit analysis is applied under small deformation assumption. Subsequently, the rigid potential sliding body $ABCDEA$ rotates around Point O with an angular velocity of Ω.

The height and the inclination angle of filler behind gravity wall at lower stage are $\alpha_1 H$ and β_1, and they are $\alpha_2 H$ and β_2 behind the anchoring frame beam at upper stage. The width of platform is represented by d. The position of the i^{th} anchor is expressed by z_i, which refers to the vertical distance between the anchor head and Line BC. The anchorage angle of anchor is ξ. Based on the associated flow rule, the logarithmic spiral line AB is a velocity discontinuity. When the soil is in a plastic flow state, the dilation angle along the failure surface is equal to the internal friction angle of soil φ. Based on the framework of upper bound analysis theorem, the rigid plastic soil mass obeys Mohr-Coulomb criterion and associated flow rule. Besides, the seismic loading is simplified as horizontal and vertical inertial forces according to pseudo-static method. The vertical seismic acceleration coefficient (k_v) can be expressed as a proportional ratio α of the horizontal seismic acceleration coefficient (k_h), thus $k_v=\alpha k_h$. It is assumed that the parameters of soil mass (cohesion c, internal friction φ and unit weight γ, friction angle with the gravity wall δ) are not influenced by seismic loading, and the self-weight of combined retaining structure is negligible.

3. The plastic limit equilibrium state

When the external power of combined retaining structure equals to the internal energy dissipation, the rigid plastic soil body $ABCDEA$ begins to slide along the potential failure surface, which is regarded as a limit state based on the upper bound method of limit analysis. The external power is mainly induced by external forces including the soil gravity W, the horizontal seismic loading k_hW, the vertical seismic loading k_vW and the seismic active earth pressure P_a. Based on the concept of pseudo-static method, the resultant force of soil gravity and vertical seismic loading can be express as $(1-k_v)W$ with a vertical downward direction. Thereafter, the external power consists of the power induced by the vertical resultant force (E_v), the power of horizontal seismic loading (E_h), and the power of seismic active earth pressure (E_a). On the other hand, the internal energy dissipation is composed of the power of anchor force (E_T) and the energy dissipation along the potential failure surface AB (E_c) and the interface between the gravity wall and the soil slope AE (E_f). Subsequently, the limit state of combined retaining structure can be expressed as

$$E_h + E_v + E_a = E_T + E_c + E_f \tag{1}$$

3.1 External power

The power induced by the vertical resultant force of rigid soil body $ABCDEA$ (E_v) is regarded as a superposition of the powers caused by the vertical resultant forces of Areas OAB, OAE, ODE, OCD and OBC (see Fig. 1). The power caused by the vertical resultant force of Area OAB can be determined as a integration of the vector product between vertical resultant force and velocity at the barycenter for each micro-element in polar coordinate. The power induced by the vertical resultant force of the other areas (OAE, ODE, OCD and OBC) can be deduced as a vector product of the vertical velocity at the barycenter and the vertical resultant force of soil. Subsequently, the power induced by the vertical resultant force of each area (E_{vm}) can be expressed as

$$E_{vm} = (1-k_v)\gamma R_0^3 \Omega \cdot f_m \ (m=0, 1, 2, 3, 4) \tag{2}$$

In which, k_v refers to the vertical seismic coefficient; f_m are parameters related to Areas *OAB*, *OAE*, *ODE*, *OCD* and *OBC* respectively when m changes from 0 to 4. The expressions of f_m (m=0, 1, 2, 3, 4) are functions of θ_0 and θ_h which are shown in 'Appendix'.

Subsequently, the power induced by vertical resultant force (E_v) is presented as

$$\begin{aligned} E_v &= (1-k_v)\gamma R_0^3 \Omega \cdot (f_0 - \sum_{n=1}^{4} f_m) \\ &= (1-k_v)\gamma R_0^3 \Omega \cdot F_0 \end{aligned} \tag{3}$$

Similarly, the power of horizontal seismic loading (E_h) can be derived as

$$\begin{aligned} E_h &= k_h \cdot \gamma R_0^3 \Omega \cdot (g_0 - \sum_{n=1}^{4} g_m) \\ &= k_h \cdot \gamma R_0^3 \Omega \cdot G_0 \end{aligned} \tag{4}$$

In which, g_0~g_6 are all the function of θ_0 and θ_h corresponding to Areas *OAB*, *OAE*, *ODE*, *OCD* and *OBC* respectively, which are shown in 'Appendix'.

The position of the resultant of seismic earth pressure on gravity wall (P_a) is assumed at 1/3 of wall height, so the power of seismic active earth pressure (E_a) can be deduced by a vector product between the velocity at this position and the resultant of seismic earth pressure (P_a), which can be expressed as

$$E_a = P_a R_0^2 \Omega \cdot p \tag{5}$$

In which, p is a function of θ_0 and θ_h which can be deduced as following according to whether the sum of the slope angle at lower stage (β_1) and the frictional angle between soil mass and gravity wall (δ) is larger than 90° or not.

$$p=\begin{cases} \sin(\beta_1+\delta)(e^{(\theta_h-\theta_0)\tan\phi}\sin\theta_h - \dfrac{\alpha_1}{3}\dfrac{H}{R_0}) \\ -\cos(\beta_1+\delta)(e^{(\theta_h-\theta_0)\tan\phi}\cos\theta_h + \dfrac{\alpha_1\cot\beta_1}{3}\dfrac{H}{R_0}) & (\delta+\beta_1 \le 90°) \\ \sin(\beta_1+\delta)(e^{(\theta_h-\theta_0)\tan\phi}\sin\theta_h - \dfrac{\alpha_1}{3}\dfrac{H}{R_0}) \\ +\cos(\beta_1+\delta)(e^{(\theta_h-\theta_0)\tan\phi}\cos\theta_h + \dfrac{\alpha_1\cot\beta_1}{3}\dfrac{H}{R_0}) & (\delta+\beta_1 > 90°) \end{cases} \tag{6}$$

3.2 Internal energy dissipation

Anchor force is used to transmit the earth pressure behind frame beam to a deep strata. Since the pull-out failure mode is widely observed subjected to seismic loading, the resistance of anchor is always regarded as the ultimate pull-out capacity of anchor. Subsequently, the pull-out failure is considered here. In this study, the seismic anchor force refers to the ultimate pull-out capacity of anchor subjected to seismic loading. According to the geometric relationship between the anchorage angle of anchor ξ and the rotation angle θ_i, the item of $R_0 e^{(\theta_i-\theta_0)\tan\varphi}\cdot\sin|\theta_i-\xi|$ that contains the unknown coefficient θ_i can be transformed to a polynomial only containing θ_0 and θ_h, which is expressed as

$$\begin{aligned} & R_0 e^{(\theta_i-\theta_0)\tan\varphi}\cdot\sin|\theta_i-\xi| \\ &= \left|\sin\xi\left[z_i\cot\beta_2 - R_h\cos\theta_h - d - \sum_{m=1}^{2}\alpha_m H\cot\beta_m\right] + \cos\xi(z_i + R_0\sin\theta_0)\right| \\ &= \left|\sin\xi\left[z_i\cot\beta_2 - (H/R_0)^{-1} H\cdot e^{(\theta_h-\theta_0)\tan\varphi}\cos\theta_h - d - \sum_{m=1}^{2}\alpha_m H\cot\beta_m\right]\right. \\ &\quad \left. + \cos\xi\left(z_i + (H/R_0)^{-1} H\sin\theta_0\right)\right| \end{aligned} \tag{7}$$

The power induced by anchor force (E_T) is a vector product between the anchor force T_i and the velocity at the potential sliding surface *AB* with a polar angle of θ_i, which is derived as

$$E_T = \sum_{i=1}^{n} T_i \cdot R_0 e^{(\theta_i-\theta_0)\tan\varphi}\cdot\Omega\cdot\sin|\theta_i-\xi| \tag{8}$$

The energy dissipation along the velocity discontinuity (E_c) can be determined as an integration along the potential sliding surface *AB* between the soil cohesion and the tangent velocity, which is presented as

$$\begin{aligned} E_c &= \int_{\theta_0}^{\theta_h} c\cdot V\cos\varphi\cdot\frac{R\cdot d\theta}{\cos\varphi} \\ &= cR_0^2\Omega\cdot\frac{e^{2(\theta_h-\theta_0)\tan\varphi}-1}{2\tan\varphi} \end{aligned} \tag{9}$$

The adhesive force between soil mass and gravity wall P_f is determined by $cl\tan\delta/\tan\varphi$ (Soubra 2000), and its action-point is in the middle of gravity wall. In which, l refers to the length of Line *AE* (along the back of gravity wall, as shown in Fig. 1). The energy dissipation induced by adhesive force (E_f) is a vector product between the velocity at the middle point of gravity wall and the adhesive force, which is expressed as following

$$E_f = cR_0^2\Omega\cdot q \tag{10}$$

In which, q is a function of θ_0 and θ_h, which is expressed as

$$q = \frac{H}{R_0}\frac{\alpha_1\tan\delta\sin(\beta_1+\theta_h)e^{(\theta_h-\theta_0)\tan\varphi}}{\sin\beta_1\tan\varphi} \tag{11}$$

4. Seismic anchor force and active earth pressure

Inverse construction measure is widely applied to support a multi-stage slope by retaining structure with a construction sequence from top to bottom. The anchoring frame beam at upper stage is constructed firstly, and the gravity wall at lower stage is constructed next. Based on the construction sequence of inverse measure, the minimum seismic anchor force of anchoring frame beam can be derived by assuming the slope at upper stage as a one-stage slope. Moreover, the seismic active earth pressure can be determined by substituting the seismic anchor force into the two-stage analytical model of combined retaining structure.

Table 1 Comparison between proposed method and existing method

H (m)	β (°)	k_h (g)	k_v (g)	c (kPa)	φ (°)	γ (kN/m^3)	S_x (m)	ζ (°)	Safety factor (F_s)		
									Cai *et al*. (2003)	Bishop (1955)	Proposed method
8	45	0	0	12	20	20	1.5	\	1.090	1.084	1.212

Table 2 Comparison between presented method and the proposed method

Case	H (m)	β (°)	k_h (g)	k_v (g)	c (kPa)	φ (°)	γ (kN/m^3)	S_x (m)	ζ (°)	F_s	Axial anchor force（kN）		
											Yan *et al*. (2019)	Proposed method	Deviation (%)
1	10	60	0.2	0.1	12	25	18	3	20	1.245	100.0	108.4	8.40
2	10	60	0.2	0.1	12	25	18	3	20	1.202	90.0	93.9	4.33
3	10	60	0.2	0.1	12	25	18	3	20	1.146	80.0	81.8	2.25

By substituting Eqs. (2)-(11) into Eq.(1), the formula of plastic limit equilibrium containing the seismic anchor force T_i and the seismic active earth pressure P_a can be deduced by taking the horizontal spacing of anchor S_x into consideration

$$(1-k_v)\gamma R_0^3\cdot F_0+k_h\cdot\gamma R_0^3\cdot G_0+P_aR_0^2\cdot p = cR_0^2\cdot\frac{e^{2(\theta_h-\theta_0)\tan\varphi}-1}{2\tan\varphi}+cR_0^2\cdot q+\sum_{i=1}^{n}\frac{T_i}{S_x}R_0\sin(\theta_i-\zeta)\times e^{(\theta_i-\theta_0)\times\tan\varphi} \quad (12)$$

4.1 The seismic anchor force

The analytical model of combined retaining structure can be simplified as a single-stage slope supported by anchoring frame beam when α_1=0, d=0, β_1=0, H_{II}=$\alpha_2 H$, f_1=f_2=0 and g_1=g_2=0. It is assumed that there are n rows of anchor with a same anchor force. Subsequently the solution of the seismic anchor force is deduced as following

$$(1-k_v)\gamma R_0^3\cdot F_0+k_h\cdot\gamma R_0^3\cdot G_0+P_aR_0^2\cdot p = cR_0^2\cdot\frac{e^{2(\theta_h-\theta_0)\tan\varphi}-1}{2\tan\varphi}+cR_0^2\cdot q+\sum_{i=1}^{n}\frac{T_i}{S_x}R_0\sin(\theta_i-\zeta)\times e^{(\theta_i-\theta_0)\times\tan\varphi} \quad (13)$$

Since the potential sliding surface AB is determined by θ_0 and θ_h, the seismic anchor force can be optimized subject to the following conditions: 0<θ_0<180° and θ_0<θ_h<180°. Based on the global optimization algorithm, the seismic anchor force can be derived by using MATLAB platform.

4.2 The seismic earth pressure

The seismic active earth pressure of gravity wall can be determined with a consideration of the anchor force at the upper-stage

$$P_a=\frac{S_xcH^2\cdot(H/R_0)^{-2}\cdot(q+\frac{e^{2(\theta_h-\theta_0)\tan\varphi}-1}{2\tan\varphi})+T\sum_{i=1}^{n}R_0e^{(\theta_i-\theta_0)\tan\varphi}\cdot\sin|\theta_i-\xi|-(1-k_v)\cdot S_x\gamma H^3\cdot(H/R_0)^{-3}\cdot F_0-k_h\cdot S_x\gamma H^3\cdot(H/R_0)^{-3}\cdot G_0}{p\cdot H^2\cdot(H/R_0)^{-2}S_x} \quad (14)$$

Similarly, the upper bound solution of the seismic active earth pressure can be obtained through the global optimization algorithm by assuming that $\partial P_a/\partial\theta_0=0$ and $\partial P_a/\partial\theta_h=0$ (0<θ_0<180° and θ_0<θ_h<180°).

5. Comparison and verification

Comparison 1. The proposed method is derived based on a two-stage slope supported by a gravity wall combined with anchoring frame beam. The solution is also applicable for a single-slope supported by an anchoring frame beam (i.e., the upper stage). Cai *et al*. (2003) established a three-dimensional finite element model of a soil slope to calculate the its safety factor, and the result is compared with conventional Bishop's simplified method (1955) for an idealized one-stage slope without any anchor. The safety factor (F_s) determined by Cai's method is 1.090 while it is 1.084 by Bishop's simplified method. The parameters of the slope are listed below: H=8 m, β=45°, k_h=0, k_v=0, c=12 kPa, φ=20°, γ=20 kN/m^3, S_x=1.5 m and ζ=15°. Based on the above information, the safety factor of slope can be determined by combining the proposed method and the strength reduction technique, as shown in Table 1. The safety factor determined by proposed method is 1.212, which is close to the solution of existing methods.

Comparison 2. The pull-out capacity of anchor under earthquake loading is compared with the result of Yan *et al.* (2019), where the safety factor (F_s) of an one-stage slope reinforced by anchors is estimated by limit analysis and pseudo-dynamic method. In which, a specific case is considered (named Condition *A*) where the time-dependent characteristic of axial anchor force is ignored under seismic excitation. The main parameters in this case are listed below: H=10 m, β=60°, k_h=0.2, k_v=0.1, c=12 kPa, φ=25°, γ=18 kN/m^3, S_x=3 m and ζ=20°. The values of axial anchor force are 100.0 kN, 90.0 kN and 80.0 kN when the safety factors are 1.245, 1.202 and 1.146 respectively in Condition *A*. The cohesion and friction angle of soil mass are reduced by safety factor according to strength reduction method. By substituting the reduced strength parameters of soil mass into the proposed method, the pull-out capacity of anchors can be calculated, as shown in Table 2. The result of axial anchor force determined by proposed method is consistent with that obtained by Yan *et al.* (2019) with the maximum deviation of only 8.4%, which is acceptable in engineering practice.

Table 4 The variance analysis of seismic anchor force and seismic active earth pressure based on orthogonal design

Item	The sum of deviation squares (×10^5)		Freedom degree f	Average value of the sum of deviation squares (×10^5)		Value of F_j		Significance level	
	Anchor force	Earth pressure		Anchor force	Earth pressure	Anchor force	Earth pressure	Anchor force	Earth pressure
k_h	273.936	37.051	3	91.312	12.350	21.465	18.418	**	**
a=k_v/k_h	112.621	19.788	3	37.540	6.596	8.825	9.837	**	**
ξ(º)	11.340	1.681	3	3.780	0.560	0.889	0.836	#	#
β_1(º)	9.240	3.568	3	3.080	1.189	0.724	1.773	#	#
β_2(º)	17.930	1.467	3	5.977	0.489	1.405	0.729	#	#
d/m	2.191	0.389	3	0.730	0.130	0.172	0.193	#	#
α_1	25.437	3.692	3	8.479	1.231	1.993	1.835	#	#
Error	178.669	28.163	42	4.254	0.671	/		/	
Total	634.769		63	/		/		/	

Table 3 Four levels of seven parameters in orthogonal design experiment

Level	k_h	a=k_v/k_h	ξ(º)	β_1(º)	β_2(º)	d/m	α_1
I	0.1	1/3	15	60	30	1	0.40
II	0.2	1/2	20	70	45	2	0.45
III	0.4	2/3	30	80	60	3	0.50
IV	0.6	1	40	90	75	4	0.60

6. Parameter analysis

To provide some suggestions for the seismic design of gravity wall combined with anchoring frame beam, the influence of main factors is analyzed based on orthogonal test, regarding horizontal seismic acceleration coefficient (k_h), ratio of vertical and horizontal seismic acceleration a(k_v/k_h), anchorage angle of anchor ξ, slope angles β_1 and β_2, width of platform d, the height coefficient of the lower stage slope α_1. In which, the slope angle of lower stage β_1 and width of platform d are the two parameters that affect the seismic earth pressure. The number of test will be extremely large when each level of each parameter is combined with each other. Subsequently, an orthogonal experiment is designed and the representative items are selected based on orthogonality. 64 sets of orthogonal test are designed corresponding to 4 levels for 7 parameters, as shown in Table 3. Some fixed parameters are listed below: c=6.2kPa, φ=34°, F_s=1.0, γ=19.6kN/m^3, H=12m, S_x=4m, δ=17°, ξ=15°.

To determine the significance level of seven parameters, the test data are analyzed by variance analysis method. Variance analysis provides a quantitative estimation of the significance level of parameters by taking the experimental error into consideration. The sum of deviation square of all test data S_T^2 consists of the sum of deviation square of each parameter S_P^2 and the sum of deviation square of experimental error S_E^2. The mathematical expressions of S_T^2, S_P^2 and S_E^2 are listed as following.

$$S_T^2 = \sum_{i}^{64} (y_i - \overline{y})^2 \tag{15}$$

$$S_p^2 = \sum_{j=1}^{7} S_j^2 \tag{16}$$

$$S_j^2 = \frac{1}{16}\sum_{l=1}^{4} K_{lj}^2 - \frac{1}{64}\left(\sum_{i=1}^{64} y_i^2\right) \tag{17}$$

$$S_E^2 = S_T^2 - S_p^2 \tag{18}$$

Where, S_j^2 refers to the deviation square of the j^{th} parameter; K_{lj}^2 refers to the square of the sum of test result at level l in the j^{th} column; y_i and $\overline{y}$ present the i^{th} test result and the average value of the test results.

In orthogonal experiment, the total freedom f_{total} is 63 which is determined by taking the test number minus unity. The freedom of specific parameter f_j =3, which equals to the number of parameter levels minus unity. Besides, the freedom of experimental error f_E is deduced by f_{total} minus the sum of f_j. The average value of the sum of deviation square corresponding to each parameter and experimental error is calculated by dividing the freedom into a sum of deviation square. The mathematical expressions for each parameter and experimental error are expressed as Eqs.(19) and (20).

$$V_j = \frac{S_j^2}{f_j} \tag{19}$$

$$V_E = \frac{S_E^2}{f_E} \tag{20}$$

Where, V_j and V_E present the average value of the sum of deviation square corresponding to the j^{th} parameter and experimental error respectively.

The value of F_j is defined as V_j/V_E, which represents the significance level of each parameter. The variance analysis of test result is shown in Table 4. Consequently, the significance sequence of those 7 parameters on seismic anchor force is: k_h, a, α_1, β_2, ξ, β_1, d. Similarly, the significance sequence on seismic active earth pressure is: k_h, a, α_1, β_1, ξ, β_2, d. The critical values of significance for each parameter ($F_{0.99}(f_j, f_E)$, $F_{0.95}(f_j, f_E)$, $F_{0.90}(f_j, f_E)$)

Table 5 Average value of each level corresponding to each parameter in the orthogonal experiment

Parameters	Item	Level			
		I	II	III	IV
k_h	Anchor force	139.816	159.105	451.905	1689.265
	Earth pressure	144.140	169.651	284.859	721.404
$a=k_v/k_h$	Anchor force	145.549	314.272	636.000	1244.270
	Earth pressure	143.965	197.417	344.821	593.851
ξ(º)	Anchor force	563.805	632.429	755.785	388.072
	Earth pressure	352.392	307.640	369.409	250.614
β_1(º)	Anchor force	786.523	518.509	476.399	558.660
	Earth pressure	436.690	275.662	251.820	315.881
β_2(º)	Anchor force	342.198	538.492	796.185	663.216
	Earth pressure	276.123	290.786	385.440	327.704
d/m	Anchor force	532.057	532.733	672.169	603.133
	Earth pressure	308.224	313.034	326.245	332.551
α_1	Anchor force	66.186	545.953	677.412	875.459
	Earth pressure	146.417	319.750	366.142	415.836

are 4.285, 2.827, 2.219 respectively, which can be figured out from the test critical value table of F-distribution. Commonly, when $F_j > F_{0.99}(f_j, f_E)$, the influence of parameter is regarded as highly significant, which is noted as '**'. When $F_{0.99}(f_j, f_E) > F_j > F_{0.95}(f_j, f_E)$, the influence of parameter is regard as significant (marked as '*'). Under the condition that $F_{0.95}(f_j, f_E) > F_j > F_{0.90}(f_j, f_E)$, the influence is less significant and signed by '*'. If $F_{0.90}(f_j, f_E) > F_j$, the parameter is regarded as less significant, which is marked as '#'. In conclusion, the significance sequence on seismic anchor force and seismic active earth pressure is almost the same. Besides, the influence of horizontal seismic coefficient on seismic anchor force and seismic active pressure is more significant than other parameters.

The average value of seismic anchor force and seismic active pressure at each level of parameter in orthogonal experiment is shown in Table 5. It is seen that the anchor force and seismic active earth pressure increase significantly as the height coefficient of lower-stage α_1 increases from 0.4 to 0.6. The anchor force and seismic active earth pressure increase firstly, and then decrease with an increment of anchorage angle ξ or the width of platform d. Moreover, the anchor force and seismic active earth pressure increase generally when the slope angle at lower stage (β_1) increases, while they decrease with the increment of slope angle at upper stage (β_2). As for the seismic design of gravity wall combined with anchoring frame beam, it is recommended that the width of platform can be reduced to 1~2 m. A larger anchorage angle results in a lower value of anchor force and seismic active earth pressure.

7. Conclusions

Based on the upper bound theorem of limit analysis, the analytical model of gravity wall combined with anchoring frame beam is established. By obtaining the external power and the internal energy dissipation, the equation of plastic equilibrium is deduced to determine the seismic anchor force and the seismic active earth pressure. The results are optimized by global optimization algorithm through MATLAB platform. Moreover, the proposed method is verified by comparison with the previous method.

A four-level orthogonal test of seven parameters is designed to analyze the influence of parameters on seismic anchor force and seismic active earth pressure. The significance of parameters is sequenced by variance analysis. Horizontal seismic coefficient is regarded as the most significant parameter on seismic anchor force and the seismic active earth pressure.

It is recommended that the width of platform can be reduced to 1~2 m, and the anchors can be set with a larger anchorage angle in the seismic design of combined retaining structure. Besides, the slope height at lower stage is suggested as 40% of the total height of whole slope.

Acknowledgments

The research described in this paper was financially supported by the National Natural Science Foundation of China (Grant Nos. 51878667, 51678571, 51308551), and the Hunan Provincial Natural Science Foundation of China (Grant No. 2018JJ2517).

References

Ahmed, S.M. and Basha, B.M. (2021), "External stability analysis of narrow backfilled gravity retaining walls", *Geotech. Geol. Eng.,* **39**(2), 1603-1620. https://doi.org/10.1007/s10706-020-01580-3

Bera, A.K. (2014), "Parametric study on uplift capacity of anchor with tie in sand", *KSCE J. Civ. Eng*., **26**(12), 5022-5037. https://doi.org/10.1007/s12205-014-0114-1.

Biondi, G., Cascone, E. and Maugeri, M. (2014), "Displacement versus pseudo-static evaluation of the seismic performance of sliding retaining walls", *Bull. Earthq. Eng.*, **12**(3), 1239-1267. https://doi.org/10.1007/s10518-013-9542-4.

Bishop, A.W. (1955), "The use of the slip circle in the stability analysis of slopes", *Geotechnique*, **5**(1), 7-17. https://doi.org/10.1680/geot.1955.5.1.7.

Cai, F. and Ugai, K. (2003), "Reinforcing mechanism of anchors in slopes: a numerical comparison of results of LEM and FEM", *Int. J. Numer. Anal. Method. Geomech.*, **27**(7), 549-564. https://doi.org/10.1002/nag.284.

Chen, W.F., Giger, M.W. and Fang, H.Y. (1969), "On the limit analysis of stability of slopes", *Soils. Found.*, **9**(4), 23-32. https://doi.org/10.3208/sandf1960.9.4_23.

Das, S., Halder, K. and Chakraborty, D. (2022), "Seismic bearing capacity of shallow embedded strip footing on rock slopes", *Geomech. Eng.*, **30**(2), 123-138. https://doi.org/10.12989/gae.2022.30.2.123.

Farshidfar, N.; Keshavarz, A. and Mirhosseini, S.M. (2021), "Seismic stability of reinforced soil slopes using the modified pseudo-dynamic method", *Earthq. Struct.*, **20**(5), 473-486. https://doi.org/10.12989/eas.2021.20.5.473.

Greco, V. R. (2014), "Analytical solution of seismic pseudo-static active thrust acting on fascia retaining walls", *Soil Dyn. Earthq. Eng.*, **57**, 25-36. https://doi.org/10.1016/j.soildyn.2013.09.022.

Hong, S.W., Geum, D.H. and Seo, M. (2022), "Ultimate uplift capacity relation of plate anchor using model testing", *KSCE J. Civ. Eng.*, **26**(12), 5022-5037. https://doi.org/10.1007/s12205-022-1210-2.

Hwang, G.S. and Chen, C.H. (2011), "Analysis of cases of gravity quay wall movement during earthquakes", *Géotechnique*, **61**(3), 199-210. https://doi.org/10.1680/geot.3625.

Jo, S.B., Ha, J.G., Lee, J.S. and Kim, D.S. (2017), "Evaluation of the seismic earth pressure for inverted T-shape stiff retaining wall in cohesionless soils via dynamic centrifuge", *Soil Dyn. Earthq. Eng.*, **92**, 345-357. https://doi.org/10.1016/j.soildyn.2016.10.009.

Kang, J.G., Kim, Y.S. and Kang, G.U. (2023), "Plift capacity of single vertical belled pile embedded at shallow depth", *Geomech. Eng.* **35**(2), 165-179. https://doi.org/10.12989/gae.2023.35.2.165.

Kokusho, T. (2019), "Energy-based newmark method for earthquake-induced slope displacements", *Soil Dyn. Earthq. Eng.*, **121**, 121-134. https://doi.org/10.1016/j.soildyn.2019.02.027.

Krabbenhoft, K. (2018), "Static and seismic earth pressure coefficients for vertical walls with horizontal backfill", *Soil Dyn. Earthq. Eng.*, **104**, 403-407. https://doi.org/10.1016/j.soildyn.2017.11.011.

Lee, D.G., Lee, S.Y. and Song, K.I. (2023), "Development of stability evaluation system for retaining walls: Differential evolution algorithm-artificial neural network", *Geomech. Eng.*, **34**(3), 329-339. https://doi.org/10.12989/gae.2023.34.3.329.

Lee, J., Liu, Q. and Park, H.J. (2019), "Effect of earthquake motion on the permanent displacement of embankment slopes", *KSCE J. Civ. Eng.*, **23**(10), 4174-4189. https://doi.org/10.1007/s12205-019-1833-0.

Li, Y.X. and Yang, X.L. (2018), "Three-dimensional seismic fisplacement analysis of rock slopes based on Hoek-Brown failure criterion", *KSCE J. Civ. Eng.*, **22**(11), 4334-4344. https://doi.org/10.1007/s12205-018-3022-y.

Lian, J., Ding, X.M. and Zhang, L. (2023), "Shaking table test on seismic response of an accumulation landslide reinforced by pile-plate retaining wall based on the time-frequency analysis method", *J. Cent. South Univ.*, **30**(5), 1710-1721. https://doi.org/10.1007/s11771-023-5323-7.

Lim, H. and Jeong, S. (2020), "Effect of bedrock acceleration on dynamic and pseudo-static analyses of soil-pile systems", *Comput. Geotech.*, **126**(2), 103657. https://doi.org/10.1016/j.compgeo.2020.103657.

Lim, H., Park, J., Kim, J. and Ko, J. (2023), "Numerical study on stability and deformation of retaining wall according to groundwater drawdown", *Geomech. Eng.*, **33**(2), 195-202. https://doi.org/10.12989/gae.2023.33.2.195.

Lin, Y.L., Lu, L., Li, Y.X., Xue, Y., Feng, Z.J., Wang, Z.M. and Yang, G.L. (2020c), "On determining seismic anchor force of anchoring frame structure supporting three-stage slope", *Geomech. Eng.*, **22**(3), 265-275. https://doi.org/10.12989/gae.2020.22.3.265.

Lin, Y.L., Cheng, X.M., Yang, G.L. and Li, Y. (2018), "Seismic response of a sheet-pile wall with anchoring frame beam by numerical simulation and shaking table test", *Soil Dyn. Earthq. Eng.*, **115**, 352-364. https://doi.org/10.1016/j.soildyn.2018.07.028.

Lin, Y.L., Jin, J., Jiang, Z.H., Liu, W., Liu, H.D., Li, R.F. and Liu, X. (2022), "Seismic response of combined retaining structure with inclined rock slope", *Struct. Eng. Mech.*, **84**(5), 591–604. https://doi.org/10.12989/sem.2022.84.5.591.

Lin, Y.L., Li, Y.X., Yang, G.L. and Li, Y. (2017a), "Experimental and numerical study on the seismic behavior of anchoring frame beam supporting soil slope on rock mass", *Soil Dyn. Earthq. Eng.*, (98), 12-23. https://doi.org/10.1016/j.soildyn.2017.04.008.

Lin, Y.L., Li, Y.X., Zhao, L.H. and Yang, T.Y. (2020b), "Investigation on seismic response of a three-stage soil slope supported by anchor frame structure", *J. Cent. South Univ.*, **27**(4), 1290-1305. https://doi.org/10.1007/s11771-020-4367-1.

Lin, Y.L., Lu, L. and Yang G.L. (2020a), "Seismic behavior of a single-form lattice anchoring structure and a combined retaining structure supporting soil slope: a comparison", *Environ. Earth Sci.*, **79**(3), 78. https://doi.org/10.1007/s12665-020-8817-8.

Lu, L., Lin, Y.L., Guo, D.D., Xing, H., Zhang, Z. and Duan, J.Y. (2023), "A modified newmark block method for determining the seismic displacement of a slope reinforced by prestressed anchors", *Comput. Geotech.,* **162**, 105697. https://doi.org/10.1016/j.compgeo.2023.105697.

Motlagh, A.T., Ghanbari, A., Maedeh, P.A. and Wu, W. (2018), "A new analytical approach to estimate the seismic tensile force of geosynthetic reinforcement respect to the uniform surcharge of slopes", *Earthq. Struct*., **15**(6), 687-699. https://doi.org/10.12989/eas.2018.15.6.687.

Nian, T.K., Jiang, J.C., Wang, F.W., Yang, Q. and Luan, M.T. (2016), "Seismic stability analysis of slope reinforced with a row of oiles", *Soil Dyn, Earthq. Eng.*, **84**, 83-93. https://doi.org/10.1016/j.soildyn.2016.01.023.

Nouri, H., Fa Kher, A. and Jones, C. (2008), "Evaluating the effects of the magnitude and amplification of pseudo-static acceleration on reinforced soil slopes and walls using the limit equilibrium horizontal slices method", *Geotext. Geomembranes*, **26**(3), 263-278. https://doi.org/10.1016/j.geotexmem.2007.09.002.

Shin, H. (2023), "Static and quasi-static slope stability analyses using the limit equilibrium method for mountainous area", *Geomech. Eng.*, **34**(2), 187-195. https://doi.org/10.12989/gae.2023.34.2.187.

Soubra, A.H. (2000), "Static and seismic passive earth pressure coefficients on rigid retaining structures", *Can. Geotech. J.*, **37**(2), 463-478. https://doi.org/10.1139/t99-117.

Srikar, G. and Mittal, S. (2021), "Modified pseudo-dynamic analysis of rigid gravity retaining wall with cohesion-less backfill and uniform surcharge", *Geomech. Eng.,* **26**(5), 453-464. https://doi.org/10.12989/gae.2021.26.5.453.

Steedman, R.S. and Zeng, X. (1990), "The Influence of phase on the calculation of pseudo-static earth pressure on a retaining wall", *Géotechnique*, **40**(1), 103-112.

https://doi.org/10.1016/0148-9062(90)93144-b
Sun, C., Chai, J., Luo, T., Xu, Z. and Ma, B. (2021), "Nonlinear shear-strength reduction technique for stability analysis of uniform cohesive slopes with a general nonlinear failure criterion", *Int. J. Geomech.*, **21**(1), 06020033. https://doi.org/10.1061/(ASCE)GM.1943-5622.0001885.
Taravati, H. and Ardakani, A. (2018), "The numerical study of seismic behavior of gravity retaining wall built near rock face", *Earthq. Struct.*, **14**(2), 179-186. https://doi.org/10.12989/eas.2018.14.2.179.
Trandafir, A.C., Kamai, T. and Sidle, R.C. (2009), "Earthquake-induced displacements of gravity retaining walls and anchor-reinforced slopes", *Soil Dyn. Earthq. Eng.*, **29**(3), 428-437. https://doi.org/10.1016/j.soildyn.2008.04.005.
Yan, M., Xia, Y., Liu, T. and Bowa, V.M. (2019), "Limit analysis under seismic conditions of a slope reinforced with prestressed anchor cables", *Comput. Geotech.*, **108**, 226-233. https://doi.org/10.1016/j.compgeo.2018.12.027.
Yazdandoust, M., Jamnani, A.R. and Sabermahani, M. (2023), "Seismic evaluation of metal-strip reinforced soil walls considering the effect of wall configuration-a shaking table study", *J. Earthq. Eng.*, **27**(14), 3929-3956. https://doi.org/10.1080/13632469.2022.2091685.
Zhang, B.A., Jiang, J., Zhang, D.B. and Liu, Z. (2021), "Upper bound solution of collapse pressure and permanent displacement of 3D tunnel faces using the pseudo-dynamic method and the kinematic approach", *Geomech. Eng.*, **25**(6), 521-533. https://doi.org/10.12989/gae.2021.25.6.521.
Zhang, Z., Lin, Y., Zhang, H., He, B., Yang, G. and Xu, Y. (2024), "A field investigation on an expansive soil slope supported by a sheet-pile retaining structure", *Struct. Eng. Mech.*, **91**(3), 315-324. https://doi.org/10.12989/sem.2024.91.3.315.
Zhao, L.H., Zuo, S., Lin, Y.L., Li, L. and Zhang, Y. (2016), "Reliability back analysis of shear strength parameters of landslide with three-dimensional upper bound limit analysis theory", *Landslides*, **13**(4), 711-724. https://doi.org/10.1007/s10346-015-0604-3.
Zhong, J.H. and Yang, X.L. (2021), "Seismic stability of three-dimensional slopes considering the nonlinearity of soils", *Soil Dyn. Earthq. Eng.*, **140**(4), 106334. https://doi.org/10.1016/j.soildyn.2020.106334.

IC

Appendix 1. Expressions of f_n and g_n (n=0, 1, 2, 3, 4)

$$f_0 = \frac{1}{3\left(1+9\tan^2\varphi\right)}\cdot[(3\tan\varphi\cos\theta_h+\sin\theta_h)\cdot \mathrm{e}^{3(\theta_h-\theta_0)\tan\varphi} - 3\tan\varphi\cdot\cos\theta_0-\sin\theta_0] \tag{21}$$

$$f_1 = \frac{\alpha_2}{3}\cdot\frac{H}{R_0}\left[\cos^2\theta_0+\frac{L}{R_0}\left(\frac{L}{R_0}-2\cos\theta_0\right) - 2\cdot\frac{d}{R_0}\cdot\left(\cos\theta_0-\frac{L}{R_0}\right)\right] \tag{22}$$

$$f_2 = \frac{d}{3R_0}\left(\cos\theta_0-\frac{L}{R_0}-\alpha_2 H\cot\beta_2-\frac{d}{2R_0}\right)\left(\sin\theta_0+\alpha_2\frac{H}{R_0}\right) \tag{23}$$

$$f_3 = \frac{\alpha_2 H}{2R_0}\left[\cos^2\theta_0+\frac{L}{R_0}\left(\frac{L}{R_0}-2\cos\theta_0-\sin\theta_0\cot\beta_2\right) + \frac{1}{2}\sin 2\theta_0\cot\beta_2 - \frac{\alpha_2 H}{2R_0}\cdot\cot\beta_2\cdot\left(\cos\theta_0-\frac{L}{R_0}+\sin\theta_0\cot\beta_2\right)\right] \tag{24}$$

$$f_4 = \frac{1}{6}\cdot\frac{L}{R_0}\cdot\left(2\cos\theta_0-\frac{L}{R_0}\right)\cdot\sin\theta_0 \tag{25}$$

$$g_0 = \frac{1}{3\left(1+9\tan^2\varphi\right)}\cdot[(3\tan\varphi\sin\theta_h-\cos\theta_h)\cdot \mathrm{e}^{3(\theta_h-\theta_0)\tan\varphi}-(3\tan\varphi\cdot\sin\theta_0-\cos\theta_0)] \tag{26}$$

$$g_1 = \frac{\alpha_2}{3}\cdot\frac{H}{R_0}\left[\frac{1}{2}\sin 2\theta_0-\frac{L}{R_0}\cdot\sin\theta_0-\frac{\alpha_2}{2}\cdot\frac{H}{R_0}\cdot\cot\beta_2\left(\cos\theta_0-\frac{L}{R_0}\right) - \frac{d}{R_0}\cdot\left(\frac{\alpha_1 H}{2R_0}+\alpha_2\frac{H}{R_0}+\sin\theta_0\right)\right] \tag{27}$$

$$g_2 = \frac{d}{3R_0}\left(\sin\theta_0+\frac{\alpha_2 H}{R_0}\right)^2 \tag{28}$$

$$g_3 = \frac{\alpha_2 H}{3R_0}\left[\cot\beta_2\sin^2\theta_0+\frac{1}{2}\sin 2\theta_0-\frac{L}{R_0}\cdot\sin\theta_0 + \frac{\alpha_2 H}{2R_0}\cdot\cot\beta_2\cdot\left(\cos\theta_0-\frac{L}{R_0}+\sin\theta_0\cot\beta_2\right)\right] \tag{29}$$

$$g_4 = \frac{1}{3}\cdot\frac{L}{R_0}\sin^2\theta_0 \tag{30}$$

In which, L refers to the length of BC.

The expressions of H/R_0 and L/R_0 are shown as following:

$$H/R_0 = \sin\theta_h\cdot e^{(\theta_h-\theta_0)\tan\varphi}-\sin\theta_0 \tag{31}$$

$$L/R_0 = \cos\theta_0-\cos\theta_h\cdot e^{(\theta_h-\theta_0)\cdot\tan\varphi} - \left(\alpha_1\cot\beta_1+\alpha_2\cot\beta_2'\right)\cdot H/R_0 \tag{32}$$